Irreversible adsorption of particles after diffusing in a gravitational field

Jordi Faraudo* and Javier Bafaluy†
Departament de Física, Universitat Autònoma de Barcelona, 08 193 Bellaterra, Barcelona, Spain
(Received 28 May 1996)

In this paper we analyze the influence of transport mechanisms (diffusion and sedimentation) on the structure of monolayers of particles irreversibly adsorbed on a line. We focus our attention on the dependence of the radial distribution function $g(r)$ and the saturation coverage θ_∞ on the gravitational Péclet number N_g. First, we study the probability density of adsorption onto an available interval using approximate solutions of the transport equation and computer simulations. Combining our results with an approximate general formalism, we can obtain values of θ_∞ and the gap density, which agree with our simulations. We also show that, for large gravity, the coverage θ_∞ approaches the ballistic limit following a power law in N_g that is independent of the number of dimensions, as has been observed in simulations R. Ezzeddine, P. Schaaf, J. C. Voegel, and B. Senger, Phys. Rev. E **51**, 6286 (1995). [S1063-651X(96)10610-3]

PACS number(s): 05.60.+w, 82.70.Dd, 68.10.Jy

I. INTRODUCTION

The adsorption of particles of colloidal size (macromolecules, latexes, bacteria, etc.) from fluid suspensions to solid surfaces is a complex phenomenon of great interest. Much effort has been devoted to the study of the mechanisms involved in this process [1]. A complete description should consider the different steps involved: (i) transport of the particles from the bulk suspension toward the interface; (ii) interaction with the substrate (including the layer formed by the previously adsorbed particles); (iii) surface diffusion and desorption. For many colloidal particles, for example, some proteins [2,3] or latexes [4,5], neither surface diffusion nor desorption is observed in the time scale accessible to experiments: the particles remain immobilized after adsorption, and the process can be considered irreversible. Consequently, nonequilibrium configurations are generated and, when the surface coverage attains a given value, a *jamming* configuration is obtained, with no space available on the surface for the adsorption of new particles.

The simplest model that attempts to describe these irreversible adsorption phenomena, is the random sequential adsorption (RSA) model [6–12]. In this model, particles are sequentially added to the surface by iteration of the following algorithm: (a) a random position is selected for the addition of a new particle; (b) if the new particle overlaps any particle already adsorbed on the surface, the adsorption attempt is rejected; (c) if the new particle does not overlap any other particle, then the adsorption attempt is accepted; (d) the time necessary for the adsorption of the particle is proportional to the number of adsorption attempts. The RSA model has been extensively studied in both discrete and continuous surfaces [6]. Exact results for the kinetics, jamming coverage, and distribution functions can be obtained analytically for one-dimensional surfaces [10]; for two-dimensional surfaces one has to use approximate methods [11,12] or computer simulations [9].

Clearly, the RSA model does not consider the transport of the particles toward the surface. Instead it assumes that new particles arrive to the neighborhood of the surface with uniform probability, and then they interact with the partially covered surface on the basis of excluded volume interactions. More realistic models must consider the different transport mechanisms that are present in colloidal systems: diffusion, gravity, externally imposed flows, and hydrodynamic and double layer forces [13].

For large enough particles suspended in a fluid at rest, gravity is the dominant force: large particles sediment following a ballistic trajectory toward the surface. This situation is described by the ballistic deposition (BD) model [14,15], in which step (b) of the RSA model is modified in the following way: if the incoming particle overlaps a preadsorbed one, then it rolls down the steepest descent path until either it reaches the surface and is adsorbed, or it is trapped in a cavity over other particles, and is rejected. This model is exactly solvable for one-dimensional surfaces [15,16], and extensive approximate studies have been realized for two-dimensional surfaces [14].

In the opposite limit of very small particles, Brownian motion becomes the dominant transport mechanism. A model describing this situation is the diffusion RSA (DRSA) model [17]: the initial position of each particle is randomly chosen in a plane at a given distance of the surface, and its trajectory is simulated by using a Brownian dynamic algorithm [18]; if the particle touches the surface it adsorbs irreversibly. Furthermore, to avoid unbound Brownian trajectories, particles arriving at points too far from the surface are rejected. The simulation of this model is much more expensive computationally than the RSA model and, furthermore, it admits no exact solution even for one-dimensional surfaces. Surprisingly, the jammed state obtained is very similar to the jammed state obtained with the RSA model: very small differences appear in one-dimensional surfaces, while in two-dimensional surfaces the jamming states obtained from both models are indistinguishable with the precision of the simulations. Analytically, good approximations can be obtained for jammed one-dimensional surfaces from approximate solutions of the diffusion equation [19].

*Electronic address: jordi@ulises.uab.es
†Electronic address: javier@ulises.uab.es

For particles of general size both, the Brownian motion and gravity have to be considered. Simulation studies have been done including the gravity force in the Brownian dynamics algorithm [20]. The results show how the properties characterizing the surface structure change smoothly with increasing gravity, from the DRSA behavior in the limit of small gravity to the ballistic values in the limit of large gravity. One interesting result is that the dependence of the jamming coverage on the size of the particles seems to scale to a common curve both for one- and two-dimensional surfaces [21]. Therefore, the information obtained from one-dimensional surfaces can be relevant also to the more realistic two-dimensional ones.

Finally, any realistic model has to include the effect of the hydrodynamic interactions (HI), which become important when the particles are in the neighborhood of the surface. Simulation results [22,23] suggest that the effect of HI on global averaged quantities is small although they should be taken into account for a fine analysis of the local structure. It can be useful therefore to study simpler models that neglect hydrodynamic interactions but can be analytically solved.

Our aim in this paper is to develop an analytic approximation to the description of the adsorption of particles on one-dimensional surfaces considering the gravity force and Brownian motion and neglecting hydrodynamic interactions. To do this, we first need solutions for the transport equation in the presence of a flat adsorbing surface and many particles fixed on it. These solutions can be obtained with a sufficient approximation when only one particle is fixed on the surface. Then, a superposition approximation has to be done to study surfaces at finite coverage; this superposition has shown good results for the DRSA model [19], and in the present model it also gives good agreement with the simulations.

In Sec. II we describe the model and the analytical tools we use in detail. In Sec. III the one-particle effects are studied by approximate solution of the transport equation and computer simulation. The results of this section allow us to obtain an approximate description of the adsorbed phase that is compared with simulations in Sec. IV. Finally, Appendixes A and B show how the approximate solutions of the transport equation can be obtained.

II. DESCRIPTION OF THE MODEL

We want to study a simple model that may allow us to understand the effect on the structure of the adsorbed layer of two simple transport mechanisms, namely, diffusion and sedimentation. We consider an adsorbing surface at $z=0$ and a semi-infinite fluid in the region $z>0$. Spherical particles of radius R suspended in the fluid diffuse in the XZ plane and sediment due to the effect of a uniform gravitational field in the Z direction. If the center of a new particle arrives at the $z=0$ line, it is adsorbed irreversibly at the contact point. We assume that the bulk concentration of particles is so small that interactions between them are negligible. Consequently, each particle adsorbs independently of the other particles in the suspension, and the process can be considered as *sequential*. However, the concentration becomes large at the surface, where adsorbed particles accumulate and interact via excluded volume effects with incoming particles.

This adsorption problem can be studied in two steps: first, the transport problem for a single particle near the surface in the presence of the previously adsorbed particles has to be solved; then, the evolution of the adsorbed phase can be studied from the obtained adsorption probabilities.

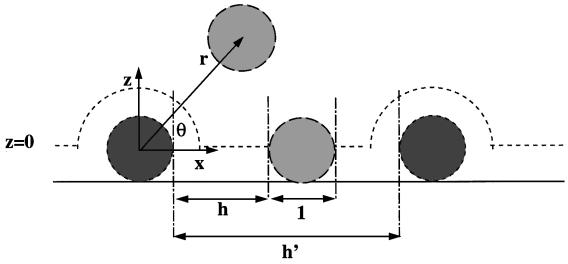

FIG. 1. Illustration of the governing equation for the nonuniform deposition.

Let $P(\vec{r},t)$ be the probability density to find the center of mass of a particle at the point $\vec{r}$ at time t; under the conditions of negligible inertia and small relaxation time, the transport of the particle to the adsorbing line is governed by the Smoluchowski equation,

$$\frac{\partial P(\vec{r},t)}{\partial t}=\vec{\nabla}\cdot[D\vec{\nabla}P(\vec{r},t)+uP(\vec{r},t)\hat{\vec{z}}], \tag{1}$$

u being the sedimentation velocity and D the diffusion coefficient assumed constant. The probability flux is given by

$$\vec{J}(\vec{r},t)=-D\vec{\nabla}P(\vec{r},t)-uP(\vec{r},t)\hat{\vec{z}}. \tag{2}$$

The hard-particle interaction between bulk particles and adsorbed ones is considered in the boundary conditions for Eq. (1) by assuming that the radial probability flux must vanish at the exclusion surface (Fig. 1) delimited by the preadsorbed particles. At the adsorbing line we impose perfectly adsorbing boundary conditions ($P=0$). Furthermore, we assume the initial condition $P(\vec{r},t=0)=\delta(z-z_0)$, z_0 being the initial distance of the center of the particle to the line; the value of z_0 is not important provided that $z_0>2R$.

Equation (1) with its boundary conditions can be made dimensionless by measuring distances in units of the diameter $2R$ of the particles and time in units of the characteristic diffusion time $\tau_{diff}=4R^2/D$. Thus, the solution of (1) depends on a single dimensionless parameter, the gravitational Péclet number N_g, defined as the quotient between τ_{diff} and the characteristic sedimentation time $\tau_{det}=2R/u$,

$$N_g=\frac{\tau_{diff}}{\tau_{det}}=\frac{2Ru}{D}=\frac{8\pi R^4 g\Delta\rho}{3k_BT}, \tag{3}$$

where g is the acceleration of gravity, $\Delta\rho$ the difference between the densities of the particles and the fluid, and T the absolute temperature. If $N_g\gg 1$ the motion of the particles is deterministic and we recover the ballistic deposition model (denoted in the following by BD), whereas if $N_g\ll 1$ Brownian motion predominates and we recover the DRSA model [19]. Note that N_g is proportional to R^4, and therefore we can define a dimensionless radius as

$$R^* \equiv R\left(\frac{4\pi g \Delta\rho}{3k_B T}\right)^{1/4} = (N_g/2)^{1/4}; \tag{4}$$

the factor 2 has been introduced to agree with the definition given in [20,21]. For polystyrene beads in water at $T=300$ K, $\Delta\rho = 45 kg/m^3$ and therefore $R^* \simeq 0.817R$ if R is expressed in micrometers. We will use these dimensionless quantities in the following.

It is not possible to analytically solve the diffusion problem (1) in the general situation, when several adsorbed particles are present. We will limit ourselves to obtaining approximate solutions in the presence of only one adsorbed particle. To describe the general situation, then, we will introduce a superposition approximation by assuming that the adsorption probability at a given point depends only on the position of the nearest particles, that is, those limiting the free interval of the line to which the point belongs. One expects this hypothesis to fail only for small gaps (and therefore only slightly affecting the layer structure) if gravity is not too high. If gravity is strong as compared to diffusion, when an incoming particle touches an adsorbed one, it is expected to adsorb in its immediate vicinity and the superposition hypothesis holds also for the smallest gaps.

According to the previous discussion, the solution of the transport equation will lead to an adsorption model in which particles are sequentially deposited onto an infinite line with an adsorption probability density that depends on the gap in which adsorption takes place. This means that the adsorbing particle only significantly interacts with the particles that are limiting this gap, and interactions with other particles are not considered. The solution of the Smoluchowski equation (1) gives the adsorption probability at any point of an available interval. The problem of characterizing the structure of the adsorbed monolayer can be studied starting from the kinetic equation for the evolution of the free gaps. We summarize the method below, and a more detailed discussion can be found in [19].

Let $G(h,t)$ be the number density of gaps with length h at time t and $k(h',h)$ the probability per unit length and per unit time that the deposition of a particle in a gap of length $h'>1$ produces gaps of length h and $h'-h-1$. The governing kinetic equation for the irreversible adsorption process is [19] (see Fig. 1):

$$\frac{\partial G(h,t)}{\partial t} = -k_0(h)G(h,t) + 2\int_{h+1}^{\infty} dh' G(h',t)k(h',h), \tag{5}$$

where $k_0(h)$ is the total rate at which gaps of length h are destroyed by the addition of a new particle:

$$k_0(h) = \int_0^{h-1} dh' k(h,h'). \tag{6}$$

The gap distribution in the jamming state can be obtained without knowing the detailed time evolution. From the balance equation (5) it is possible to derive a time-independent equation for the total number density of gaps of length h that have been created at any time along the process, $n(h)$ [19]:

$$n(h) = 2\int_{h+1}^{\infty} dh' p(h',h) n(h'), \tag{7}$$

where $p(h',h)$ is the probability density that the first particle arriving at an interval of length h' creates two new free intervals of length h and $h'-h-1$,

$$p(h',h) = \frac{k(h',h)}{k_0(h')}. \tag{8}$$

From the definition of $k_0(h)$, Eq. (6), this function satisfies the normalization

$$\int_0^{h'-1} p(h',h)dh = 1. \tag{9}$$

In addition Eq. (7) must be supplemented by a normalization condition for $n(h)$. From the definition of $n(h)$ we have [19]

$$\int_0^1 (1+h)n(h)dh = 1. \tag{10}$$

A global measure of the particle packing is the coverage defined as the relative length (area in two dimensions) of a line of total length L covered by N particles of radius R:

$$\theta = \frac{2RN}{L}. \tag{11}$$

The coverage increases monotonically (due to the irreversible nature of the process) until a saturation value θ_∞, when no available space remains for adsorption of new particles. In this situation only gaps with $h \leqslant 1$ survive and the saturation coverage can be obtained from $n(h)$ using the fact that the particle number is equal to the number of gaps,

$$\theta_\infty = \int_0^1 n(h)dh. \tag{12}$$

Let us remark that Eq. (7) expresses the fact that the total number of gaps of length h can be computed from the number of gaps with length $h'>h+1$ and the probability $p(h',h)$ of obtaining an interval of length h from an interval of length h'. In principle, from Eqs. (7)–(12) it is possible to obtain $n(h)$ and the saturation coverage θ_∞ if $p(h',h)$ is known. For each specific adsorption model $p(h',h)$ must be previously known.

In order to obtain $p(h',h)$, we must solve Eq. (1) with two adsorbed particles limiting a gap of length h' according to the hypothesis assumed in the derivation of Eqs. (5)–(7). The accuracy of this ansatz is analyzed by means of Brownian dynamics simulations in Sec. IV.

III. ADSORPTION PROBABILITY

In this section, we study the probability density of the adsorption of a new particle on a line in which one adsorbed sphere is already present. To find this probability we compute approximate solutions of the Smoluchowski equation (1) and we perform Brownian dynamics simulations. The results obtained will be used in the next section to determine

the structure and coverage of jammed lines.

To use the integral equation (7), we need the probability density $p(h',h)$ defined in (8), which can in principle be obtained by solving the Smoluchowski equation (1) in presence of two preadsorbed particles separated by a center to center distance $h'+1$. However, the solution to this problem is very difficult and therefore we have adopted a superposition hypothesis assuming that the joint effect of the two preadsorbed particles can be obtained from a superposition of the one-particle effects.

The one-particle adsorption problem is defined as follows: the center of an adsorbed particle is fixed at the point $(x,z)=(0,0)$ and, at time $t=0$, a new particle starts to move from an initial point at a given distance from the surface z_0, with a random initial value of x. The initial height z_0 is immaterial and it will be assumed to be infinite. In the presence of a nonvanishing gravity field, the particle will be adsorbed with probability one. We normalize $P(\vec{r},t)$ in such a way that the initial probability per unit length is equal to one. Therefore, the probability density of adsorption at a point of the adsorbing line $z=0$ is

$$\rho(x)=-\int_0^\infty J_z(x,z=0,t)dt, \tag{13}$$

where $J_z(x,z,t)$ is the z component of the probability flux defined in Eq. (2). Using the superposition hypothesis, we write for the probability density of adsorption on a gap of length h':

$$p(h',h)\simeq N(h')\rho(h+1)\rho(h'-h), \tag{14}$$

where $N(h')$ is determined by the normalization condition (9). To obtain $\rho(x)$ we do not need to solve the time-dependent Smoluchowski equation (1). We only need the time-integrated probability density,

$$\psi(\vec{r})=\int_0^\infty dtP(\vec{r},t), \tag{15}$$

that obeys the equation [obtained by the integration of (1) and using dimensionless units]

$$\nabla^2\psi(\vec{r})+N_g\frac{\partial\psi(\vec{r})}{\partial z}=0. \tag{16}$$

The boundary conditions satisfied by ψ are the perfect adsorbing boundary condition on the line $z=0$:

$$\psi(x,z=0)=0, \tag{17}$$

and the condition that the total probability flux coming from $z=\infty$ is 1 per unit length,

$$\frac{\partial\psi(\vec{r})}{\partial z}+N_g\psi(\vec{r})\to 1, \quad z\to\infty. \tag{18}$$

Using Eq. (13) and the boundary condition (17), $\rho(x)$ can be obtained from ψ as

$$\rho(x)=\left.\frac{\partial\psi}{\partial z}\right|_{z=0}. \tag{19}$$

Another boundary condition is necessary to account for the presence of the previously adsorbed particle in the origin of coordinates. The hard sphere interaction between diffusing and adsorbed particles implies no radial flux at the exclusion sphere (of radius $2R$) centered at the origin; therefore we have (see Fig. 1):

$$\left(\frac{\partial\psi(r,\theta)}{\partial r}\right)_{r=1}+N_g\psi(r=1,\theta)\sin\theta=0. \tag{20}$$

The solution $\psi(\vec{r})$ can be split into two parts,

$$\psi(\vec{r})=\psi^{(0)}(\vec{r})+\psi^{(1)}(\vec{r}), \tag{21}$$

where $\psi^{(0)}$ is the solution corresponding to a clean adsorption line, and $\psi^{(1)}$ reflects the presence of the adsorbed particle and must vanish at large distances. The solution of (16) for $\psi^{(0)}(\vec{r})$ with conditions (17),(18) is

$$\psi^{(0)}(x,z)=\frac{1}{N_g}(1-e^{-N_gz}). \tag{22}$$

The probability density of adsorption in the presence of the fixed particle is obtained using Eq. (19):

$$\rho(x)=\left.\frac{\partial\psi^{(0)}}{\partial z}\right|_{z=0}+\left.\frac{\partial\psi^{(1)}}{\partial z}\right|_{z=0}\equiv 1+\rho^{(1)}, \tag{23}$$

where $\rho^{(1)}$ is the deviation of ρ from the uniform distribution. In the interior of the region excluded by the fixed particle ($|x|<1$), the total flux has to be zero and therefore $\rho^{(1)}=-1$. In the available region ($|x|>1$), $\rho^{(1)}$ gives the local increase of the adsorption probability due to the particles that have been in contact with the adsorbed particle; these particles are rejected in the RSA model, but here are allowed to diffuse and will adsorb in the neighborhood of the fixed particle. The presence of the fixed particle does not change the total adsorption probability, so the integral of $\rho^{(1)}$ over the entire line has to vanish. Therefore one has

$$\int_1^\infty \rho^{(1)}dx=1. \tag{24}$$

The equation and boundary conditions for $\psi^{(1)}(\vec{r})$ can be obtained by substitution of (21),(22) in (16),(17),(20). It is not possible to obtain a solution for general values of N_g, and different approaches have to be used in the limits of small and large gravity.

A. Small gravity

We obtain a multipolar expansion for $\rho(x)$ by solving the equation for $\psi^{(1)}(\vec{r})$ and substitution in (23). To obtain $\psi^{(1)}(\vec{r})$ we use the Green function method, for the detailed calculations see Appendix A. The (formally exact) result for $\rho(x)$ can be expressed in the form

$$\rho(x)=1+\frac{2}{\pi|x|}\sum_{n=1}^{\infty}(2n-1)\varphi_{2n-1}\frac{K_{2n-1}\left(\frac{N_g}{2}|x|\right)}{K_{2n-1}\left(\frac{N_g}{2}\right)},$$

$$|x|>1, \tag{25}$$

where $K_n(x)$ is the Bessel function of third kind and the coefficients φ_{2n-1} satisfy the infinite linear system of Eqs. (A18),(A19).

By substitution of the multipolar expression (25) in (14) we obtain the probability density of adsorption on a gap of length h' for given N_g. The normalization factor $N(h')$ is obtained by numerical integration of (9). For practical uses, the series (25) must be truncated by using a finite number of terms; the larger the gravitational Péclet number N_g is, the larger the number of terms that have to be retained in (25) to achieve a given precision. We recall that if we want to obtain the saturation coverage θ_∞ we have to solve the integral equation (7) with the kernel $p(h',h)$ given by Eqs. (14),(25). If N_g is of order 1 we need only a few terms in the summation and the numerical solution of the integral equation is possible, but for intermediate to high values of N_g we need a very large number of terms and this expansion becomes useless. Therefore, it is necessary to obtain an asymptotic expression for large values of N_g to enable a description in the entire range of variation of N_g. We will return to this question in the next subsection.

We can see how the DRSA result [19] can be recovered by taking the $N_g\to 0$ limit in the previous expression. For small N_g we need only one term in (25), because $\varphi_{2n-1}=\pi/2\delta_{1n}+O(N_g)$. Therefore,

$$\rho(x)=1+\frac{1}{|x|}\frac{K_1\left(\frac{N_g}{2}|x|\right)}{K_1\left(\frac{N_g}{2}\right)}+O(N_g)\approx 1+1/x^2. \tag{26}$$

The last approximation has been obtained using the small argument expansion of the Bessel function $K_1(x)\simeq 1/x$. It gives the known zero-gravity result [19] and we see now that it gives an approximation for small gravity valid in the region $x\ll 2/N_g$.

The first moment of $\rho^{(1)}$ gives the mean distance to the origin where particles touching the fixed one adsorb. From Eq. (25), and using the well-known formula for the derivatives of Bessel functions, $K_{n-1}(y)+K_{n+1}(y)=-2K_n'(y)$ we obtain:

$$\langle|x|\rangle_1=\int_1^\infty \rho^{(1)}(x)x\,dx=\frac{2}{\pi}\sum_{n=1}^{\infty}\frac{(2n-1)\varphi_{2n-1}(N_g)}{\frac{N_g}{2}K_{2n-1}\left(\frac{N_g}{2}\right)}$$

$$\times(-1)^{n+1}\left[K_0\left(\frac{N_g}{2}\right)+2\sum_{i=2}^{n}(-1)^{i-1}K_{2i-2}\left(\frac{N_g}{2}\right)\right]. \tag{27}$$

For $N_g\to 0$ only the first term of this sum has to be retained, obtaining

$$\langle|x|\rangle_1\approx\frac{2}{N_g}\frac{K_0(N_g/2)}{K_1(N_g/2)}\approx\ln\left(\frac{4}{N_g}\right). \tag{28}$$

The mean distance increases without bound, as can be expected from the DRSA limit given by Eq. (26).

B. Large gravity

For large values of N_g one can try to solve Eq. (16) by a perturbative approach. In the $N_g\to\infty$ limit the higher order derivatives in Eq. (16) are negligible, and an approximate equation is obtained retaining only the advective term. This is equivalent to completely neglecting diffusion. The corresponding solution satisfying the boundary condition at infinity is $\psi=1/N_g$, which does not verify the boundary conditions at $z=0$ and $r=1$. The reason is that, no matter how large N_g is, diffusion becomes important near the boundaries of the system: ψ must change appreciably in a thin *boundary layer*, and the corresponding derivatives are no longer negligible in that layer.

The problem can be solved using singular perturbation techniques as discussed in Appendix B. The result is that, for large values of N_g, $\rho^{(1)}(x)$ scales to a function of the form

$$\rho^{(1)}(x)\approx N_g^{2/3}\phi^{(1)}[(x-1)N_g^{2/3}], \tag{29}$$

where function $\phi^{(1)}$ is defined in the appendix. The mean distance at which a particle that hits the preadsorbed one can be adsorbed is therefore a quantity of order $N_g^{-2/3}$

$$\langle|x|\rangle_1=\int_1^\infty\rho^{(1)}(x)x\,dx\approx 1+\frac{A}{N_g^{2/3}},$$

$$A=\int_0^\infty\phi^{(1)}(\xi)\xi\,d\xi\approx 1.106\cdots. \tag{30}$$

Obviously this distance decreases when N_g grows because diffusion is weak and the particles adsorb closer. If $N_g=\infty$, a particle hitting the fixed sphere will roll over it and be adsorbed in its immediate vicinity (at $|x|=1$) as corresponds to the rolling mechanism of BD. If N_g is large but finite, diffusion disturbs the deterministic motion and the new particle can be adsorbed at some distance from the adsorbed one, leaving between them a gap of size $h\sim N_g^{-2/3}$.

We can give a simple reasoning supporting the scaling given by Eq. (30) for large values of N_g. Particles falling over the fixed particle will roll down over it and diffuse away along a thin layer of thickness δ. This thickness can be estimated from the condition that the radial probability flux due to gravity, which is proportional to $N_g\sin\theta$, has to be compensated with the diffusion flux that can be estimated as δ^{-1}. Therefore, in dimensionless units the boundary layer thickness is

$$\delta(\theta)=\frac{1}{N_g\sin\theta}. \tag{31}$$

This thickness increases when the particle approaches the line $\theta=0$. For small angles the surface of contact between the particles becomes vertical, and the rolling picture is no longer applicable. Instead, we can imagine that particles dif-

fuse away from the fixed sphere at a certain angle, θ_0. This separation is expected to occur when the x coordinate of the center of the falling particle is beyond the region excluded by the fixed one. Given Eq. (31), this implies $[1+\delta(\theta_0)]\cos\theta_0 \simeq 1$. Solving this equation for small angles, we obtain $\theta_0 \simeq (2/N_g)^{1/3}$. From this point the incident particle falls a distance $z_0 \simeq (2/N_g)^{1/3}$; the dimensionless time needed to reach the $z=0$ line is $t_0 \simeq z_0/N_g = 2^{1/3} N_g^{-4/3}$. Due to the horizontal Brownian motion performed during the particles' falling, one expects a horizontal deviation of order $\delta x \simeq \sqrt{2t_0} \simeq (2/N_g)^{2/3}$. This simple argument gives an exponent and order of magnitude that agrees with the more exact singular perturbation result (30).

C. Brownian dynamics simulations

Computer simulation allows us to study the adsorption probability for the whole range of N_g values and to verify the validity of the results obtained in the previous subsections. The algorithm developed here will be also used in the following section to study the structure of jammed lines.

We consider, as described in Sec. II, a suspension of Brownian particles that is dilute enough to assume sequential adsorption. One by one, the center of mass of a new particles starts its motion at a fixed vertical position z_0 and at a horizontal position x_0 chosen at random from a uniform distribution. The value of z_0 does not affect the final adsorption probability as far as in the initial position there is no possibility of interaction with the adsorbed particles, that is, $z_0 > 1$. In our simulations we take $z_0 = 1$ to minimize the simulation time required.

The particle motion is discretized in time in the following way. At every time step Δt the particle develops two motions performed sequentially in the simulations. It travels a vertical distance $\Delta z_{det} = -N_g \Delta t$ (in the dimensionless units introduced in Sec. II) as corresponds to the sedimentation under gravity and a stochastic displacement $\Delta \vec{r}_{rd}$ as corresponds to the Brownian motion. Therefore,

$$\Delta \vec{r} = -N_g \Delta t \vec{z} + \Delta \vec{r}_{rd}. \tag{32}$$

As is well known, the Brownian displacement in two dimensions follows a normal distribution law with zero mean and variance

$$\langle \Delta \vec{r}_{rd}^{\,2} \rangle = 4\Delta t. \tag{33}$$

After these two motions are generated, the simulation time is increased by Δt and the algorithm is repeated until the particle reaches the adsorbing line $z=0$. The time step Δt is chosen in such a way that ensures a typical displacement of the particle to be of magnitude ϵ which is small compared to the particle diameter, $\epsilon \ll 1$. The typical Brownian displacement is of order $\sqrt{\Delta t}$, so $\Delta t \leqslant \epsilon^2$. On the other hand, the deterministic displacement is $-N_g \Delta t$, so $\Delta t \leqslant \epsilon / N_g$. Therefore, we impose

$$\Delta t = \min[\epsilon^2, \epsilon/N_g]. \tag{34}$$

The value of ϵ is restricted by computer time limitations. All the simulations reported in this paper were obtained with $\epsilon = 0.05$.

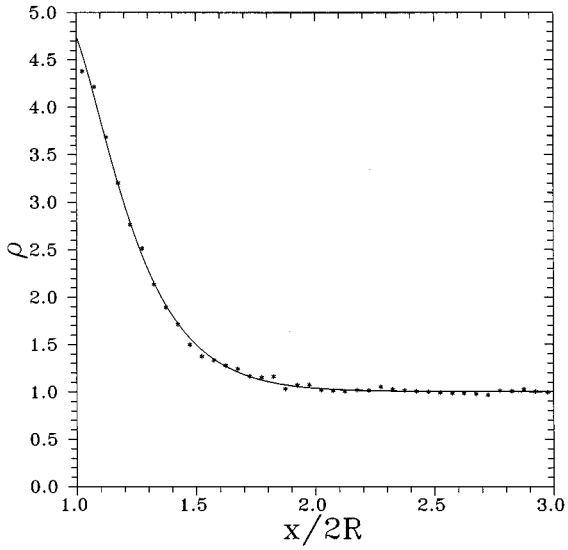

FIG. 2. Probability density of adsorption in presence of a preadsorbed particle as a function of distance for $N_g = 10$. Solid line: multipolar solution of transport equation (25) including five terms. Dots: Brownian dynamic simulations.

To complete the simulation algorithm, we need a collision rule to use in the case that an incoming particle touches the preadsorbed one. We consider two collision rules, depending on whether at the collision instant the particle is performing a deterministic or a random displacement. If the collision occurs during the deterministic displacement, we consider that the incoming particle rolls over the preadsorbed one. The collision rule for the Brownian motion is a perfect reflection of the particle trajectory, as in an elastic collision with an infinitely massive particle. This rule is an approximation, valid if the Brownian displacement is sufficiently small in relation to the radius of the boundary.

When the center of the particle reaches the $z=0$ line, we consider that the particle adsorbs at the contact point, which is recorded. By iteration of this algorithm one obtains a histogram of adsorption frequencies as a function of the distance to the fixed particle.

For small values of N_g the results obtained by Brownian dynamics simulations agree with the analytical results obtained from the superposition approximation, Eq. (14), and the multipolar expansion, Eq. (25), see Fig. 2. For large values of N_g the simulated distribution of adsorbed particles approaches the scaling (29) predicted by the asymptotic approximation, see Fig. 4.

To obtain a simple analytic approximation in the intermediate to high N_g regime, we fit the simulation results for $\rho(x)$ with an exponential distribution,

$$\rho(x) \simeq 1 + b e^{-b(|x|-1)}, \quad |x| > 1. \tag{35}$$

Although the asymptotic form of the adsorption probability obtained in Appendix B is not exactly an exponential, this is a simple fitting function. To determine the value of $b(N_g)$ from the simulation results we impose the condition that the thickness of the exponential has to be equal to the thickness

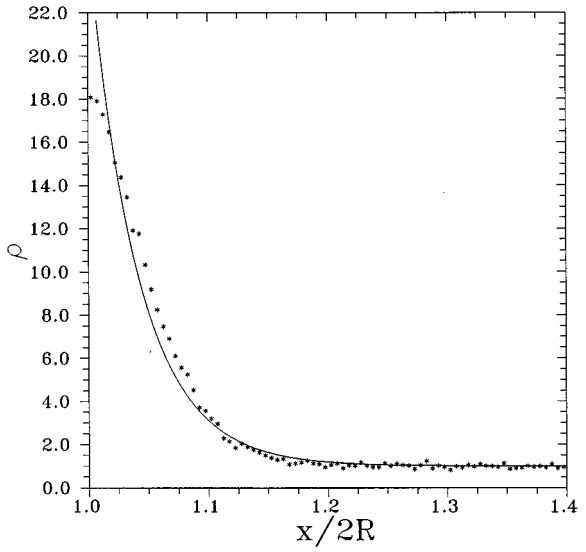

FIG. 3. Probability density of adsorption in the presence of a preadsorbed particle as a function of distance for $N_g=60$. Solid line: exponential distribution (35). Dots: Brownian dynamic simulations.

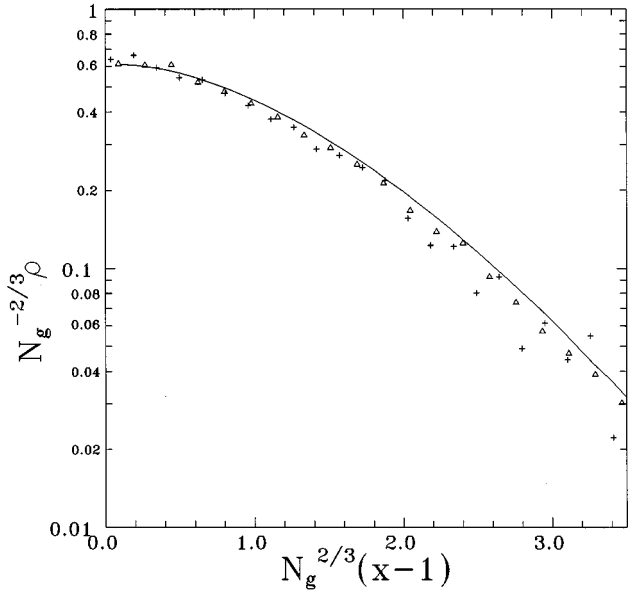

FIG. 4. Logarithmic of the scaled probability density of adsorption in the presence of a preadsorbed particle. Simulation results for $N_g=60$ (crosses) and $N_g=300$ (triangles). Continuous line: Numerical solution of boundary layer equation.

of $\rho^{(1)}$ obtained from the simulations. This is the condition of maximum likelihood for an exponential distribution [28], and it implies

$$\frac{1}{b}=\langle|x|\rangle_1-1. \tag{36}$$

For large values of N_g we expect, based on our asymptotic argument (30), a dependence of the form $\langle|x|\rangle_1=1+\alpha N_g^{-2/3}$ To determine the constant α we computed the mean distance of the adsorbed particles to the previously adsorbed one for different N_g numbers. The simulations were performed for $N_g=60,80,100,140,200,400,600$ using 40 000 particles in each simulation and we obtained:

$$b=\frac{N_g^{2/3}}{\alpha},\quad \alpha=1.08\ldots, \tag{37}$$

in agreement with the value 1.106 . . . obtained from the asymptotic solution (30). In Fig. 3 we compare this exponential fit, Eqs. (35), (37), with the results of the Brownian dynamic simulations for $N_g=60$.

Making use of the superposition hypothesis (14) and the normalization condition (9) the probability density of adsorption in a gap can be expressed in the simple form:

$$p(h',h)=\frac{1+be^{-bh}+be^{-b(h'-h-1)}}{h'+1-2e^{-b(h'-1)}}. \tag{38}$$

Although the exponential distribution does not reproduce all the details of the simulated $\rho(x)$, it approaches its main characteristics, and the corresponding kernel (38) is simple enough to allow a numeric evaluation of the integral equation (7).

IV. STRUCTURE OF THE ADSORBED LAYER

In this section we present results concerning the structure of the adsorbed layer at jamming, characterized by the coverage θ_∞ and the radial distribution function $g(r)$. In Sec. IV A we study the variation of the jamming coverage with N_g and in Sec. IV B we analyze the local structure of jammed surfaces described by $g(r)$. The results obtained by numerical integration of Eq. (7) using (38) or (25) are compared with simulation results.

The characteristics of the simulations are as follows. For each value of N_g we have filled 1000 lines of length $L=100$ and we have computed the mean number of particles adsorbed at saturation. The statistical uncertainty on the coverage (error bars) is estimated by a 95% confidence interval. In principle, particle trajectories are simulated as long as the surfaces are not entirely covered, but there exist some special cases that demand more attention to avoid prohibitive computer time. Consider a particle diffusing in the region between two preadsorbed ones, being the interval of the line between these preadsorbed particles of length less than 1. This particle only can adsorb if it obtains sufficient thermal energy to overcome the gravitational force and the geometrical barrier delimited by the preadsorbed particles. The time needed to escape from these ''geometrical barriers'' grows rapidly with N_g. For $N_g\sim1$ the particle can return to the bulk after a small time and try to adsorb elsewhere. However, for sufficiently high N_g this time becomes very large (infinite in the case of BD). In the practical situation, these particles play no role because other particles, coming from the bulk, will adsorb in the free gaps. There are different ways in which this effect can be taken into account [25]. In our simulations we adopt the following criteria: we choose a maximum residence time τ and, if a given particle remains time $t>\tau$ in a trap, it is eliminated from our simulations and a new particle starts the motion following the previous rules.

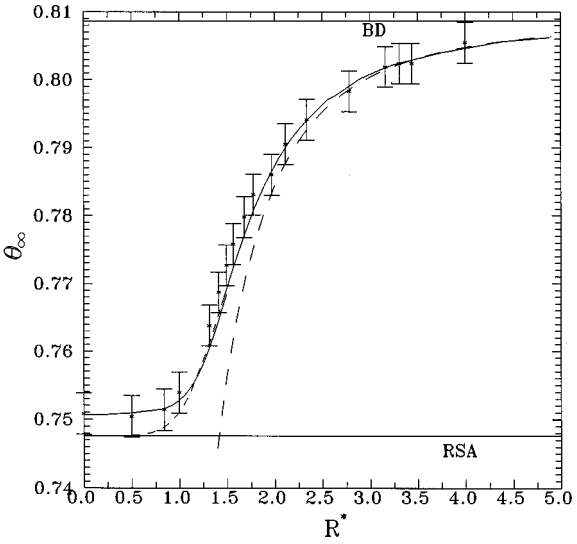

FIG. 5. Comparison between the saturation coverage θ_∞ as a function of R^* obtained with several methods. (a) Dots: Brownian dynamic simulation. (b) Solid line: numerical solution of the integral equation (7) using the multipolar solution (25) truncated to five for $R^*<1.5$ and the exponential fitting (35) for $R^*>1.5$. (c) Dashed line: asymptotic expression (39). (d) Short dashed line: continuation of the numeric solution with exponential fitting (35) for $R^*<1.5$.

We take a different characteristic residence time τ for each N_g. For small N_g only a few particles are eliminated, but for $N_g \gg 1$ usually all particles that fall into intervals of length $h<1$ are eliminated. For $R^* \leqslant 1$ we take $\tau=15$, $\tau=8$ for $1<R^* \leqslant 2$ and $\tau=1$ for $R^*>2$. We have checked that our results are not sensible to increments of τ. Finally, the last stage is simulated in the following way. When only gaps with length $h'<3$ survive, the initial position x_0 is chosen at random between the centers of the particles limiting these gaps, at $z=1$ as for the other particles. When only targets of length $h'<2$ remain (at most one particle can be adsorbed in each) we fill these by using a RSA algorithm, i.e., by randomly placing a particle in it without any transport process. Only a few particles are deposited following these two last rules and therefore the structure [characterized by $g(r)$] is not significantly altered.

A. Coverage at the jamming limit

For adsorption on an infinite line, the saturation coverage can only be a function of the unique dimensionless parameter present in the transport equation, namely, N_g. It is more convenient to represent the variation of θ_∞ as a function of the dimensionless radius, R^*, defined in Eq. (4), which gives a more compact scale than N_g.

In Fig. 5 we show the variation of θ_∞ with R^* obtained by simulation (crosses) and by solving the integral equation (7) following the numerical method described in [19]. The solid line in the region $R^*<1.5$ ($N_g \leqslant 10$) has been obtained with the kernel given by substitution of the multipolar expression (25) truncated to five terms in Eq. (14). We also solve, for all values of R^*, the integral equation (7) with the kernel obtained using the exponential approximation, Eq. (38); the result is represented by the solid line for $R^*>1.5$ and by the short dashed line for $R^*<1.5$.

Three main regions can be recognized in the graph:

(1) $R^* \leqslant 1$: In this region the Brownian motion dominates. The coverage varies slowly with R^* and its value remains close the DRSA value ($\theta_\infty \simeq 0.7506$). For example, for the $R^*=1$ case we obtain $\theta_\infty \simeq 0.7539$ by means of simulations and the numerical solution of the integral equation with the multipolar kernel yields $\theta_\infty \simeq 0.7528$. Simulation results agree with the curve obtained using the multipolar solution of transport equation. The curve obtained using the exponential kernel (38) gives smaller values for θ_∞ and in the limit of vanishing gravity it approaches the RSA coverage $\theta_\infty \simeq 0.747\,59\ldots$ instead of the DRSA value.

(2) $1 \leqslant R^* \leqslant 2.5$: θ_∞ rises quickly with R^*. In this region the numerical solutions of the integral equation with the multipolar expression and with the exponential approximation (38) are close. However, they show a slight discrepancy with the simulation results that are systematically greater.

(3) $R^* \geqslant 2.5$ θ_∞ approaches slowly to the BD limit ($\theta_\infty^{BD}=0.808\,65\ldots$), for example, if we take $R^*=10$ ($N_g=10^4$) simulations give $\theta_\infty=0.807\ldots$. We obtain good agreement between the simulations and the solution of (7) using the exponential kernel (38). A simple expression describes the asymptotic approach to the strong gravity limit, $N_g \to \infty$:

$$\theta_\infty(N_g \gg 1) \simeq \theta_\infty^{BD} - 0.2445 N_g^{-2/3}. \tag{39}$$

This expression is shown in Fig. 5 by dashed lines, and can be obtained considering a simplified model. For large values of N_g, the explicit form of $\rho^{(1)}$ seems not to be of great importance provided that it gives a value for the mean distance between the adsorbed particles and the preadsorbed one in agreement with Eq. (30). We can use instead of the exact density, an approximation in which $\rho^{(1)}$ is described by a normalized step function of thickness $2\langle|x|\rangle_1 = 2AN_g^{-2/3}$ in agreement with (30). This model is exactly solvable [24], giving (39) in the limit $N_g \to \infty$.

We have performed some control simulations to study the origin of the slight discrepancy between the solid line and simulations in region 2 on the graph. This effect is due to the fact that for this range of N_g the probability density of adsorption on a gap not only depends on the gap's limiting particles but can also be influenced by third neighbors. This can be clearly shown by performing simulations with three preadsorbed spheres and comparing the resulting adsorption density probability with the result of the superposition approximation (14). In Fig. 6 we show the adsorption probability density in a situation with three pre-adsorbed spheres on a line of length $L=20$ and $R^*=1$. Between spheres one and two there is a gap of length $h'=2.5$ and between spheres two and three there is a small gap of $h'=0.05$ that does not allow particle adsorption therein. Simulation results show an asymmetric adsorption probability, which clearly displays the effect of the third particle. The solution corresponding to the superposition hypothesis (14), which assumes that the adsorption probability in one gap is given by the product of the one-particle solutions corresponding to the particles at the ends of the interval, shown in the continuous line, is symmetric. We also note that the simulation results fit well with a distribution constructed as a product of the three one-

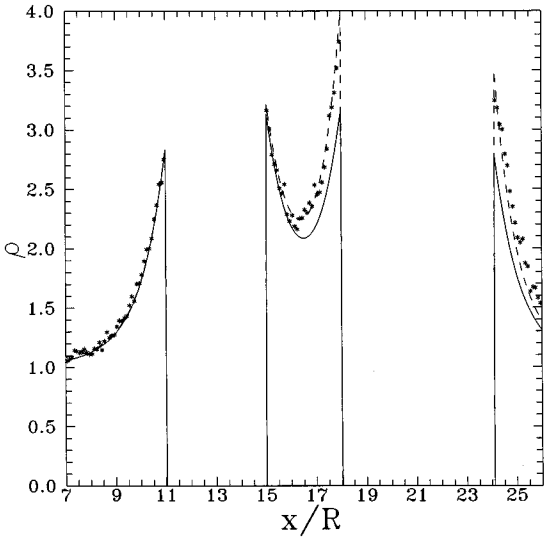

FIG. 6. Probability density of adsorption in a line of length $40R$ in the presence of three adsorbed particles, at positions $x_1=13R$, $x_2=20R$, $x_3=22.1R$. (a) Dots: Brownian dynamic simulations. (b) Solid line: superposition of the two one-particle solutions corresponding to the particles limiting each gap. (c) Dashed line: Superposition of the three one-particle solutions.

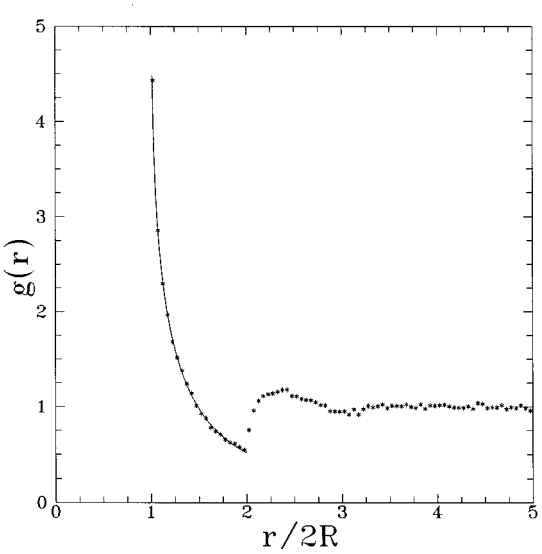

FIG. 7. Radial distribution function $g(r)$ for $R^*=1$. Dots: Brownian dynamic simulations. Solid line: Calculation of $g(r)$ for $1\leqslant r\leqslant 2$ using the numerical solution of the integral equation (7) for $n(h)$.

particle solutions (dashed line). For larger R^* values, the ansatz of independence of gaps holds, and the theoretical expression shows no significant deviation from their simulation counterpart.

B. Radial distribution function at the jamming limit

The radial distribution function, $g(r)$, reflects the correlation existing between the adsorbed particles. The definition adopted here is the usual one in statistical mechanics (see, for instance, [26]). In this subsection, we present histograms of $g(r)$ in the jamming limit, obtained from the Brownian dynamic simulations used in the previous subsection to determine θ_∞.

In Figs. 7 and 8 we show $g(r)$ for various values of R^*. At the jamming limit, $g(r)$ presents a logarithmic singularity at $r=1$, like the RSA model. The simulation results, however, are histograms that have a finite value at contact representing an average of $g(r)$ over a finite distance interval. This contact value is nearly constant for $R^*\leqslant 1$ whereas it grows with R^* for $R^*>1$.

For $R^*\leqslant 1$ our $g(r)$ are indistinguishable from the results obtained for DRSA ($R^*=0$). The $g(r)$ for $R^*=1$ is shown in Fig. 7; note the disappearance of correlations between particles after a few diameters. We recall that the variation of θ_∞ with R^* in this region is less than 1%, as we pointed out in the previous section. Therefore, we can conclude that for $R^*\leqslant 1$ the structure of the adsorbed layer is almost independent of gravity.

In Fig. 8 we show the radial distribution function for $N_g=30$ ($R^*=1.968$) and for $N_g=240$ ($R^*=3.310$). A comparison between Figs. 7 and 8 shows that peaks in $g(r)$ increase and are steeper as R^* increases, revealing the tendency of large particles to pack closer together than smaller ones. This is because diffusion is a small effect for large particles, and there is an increased probability of adsorption close to already adsorbed particles. We can observe that the smaller the effect of gravity (as measured by R^*), the poorer the structure in the radial distribution function. For $1\leqslant R^*\leqslant 2.5$ not only the coverage changes rapidly with R^* (as noted in Sec. IV A) but $g(r)$ does also. Note for example that, for $R^*=1.968$, two secondary peaks are visible whereas only one is visible for $R^*=1$. For $R^*>2.5$ the obtained $g(r)$ are very close to the correlation function of the ballistic deposition model, although the δ function singularities present in the BD model at $r=1,2,\ldots$ are smoothed due to the effect of diffusion. Our model differs from other

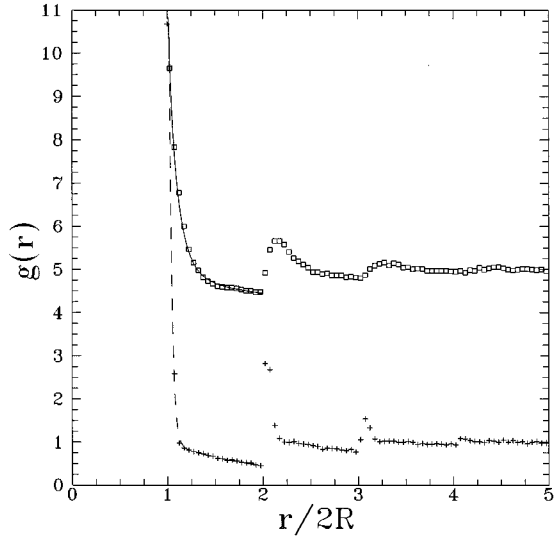

FIG. 8. Simulation results for $g(r)$ corresponding to $R^*=1.968$ ($N_g=30$), squares and $R^*=3.310$ ($N_g=240$) displaced four units, crosses. Solid line: Calculation of $g(r)$ for $1\leqslant r\leqslant 2$ and $N_g=30$ using the numerical solution of the integral equation (7). Dashed line: the same for $N_g=240$.

generalized models [16] in which the δ funciton singularities appear only for $R^*=\infty$.

At the jamming limit $g(r)$ cannot be obtained completely using the formalism presented in Sec. II, but it can be obtained for $1\leqslant r\leqslant 2$ noting that $n(h)$ is equal to $g(h+1)$ for $0\leqslant h\leqslant 1$ except by the normalization. By the definition of these functions one has

$$n(h)=\theta_\infty^2 g(h+1), \quad h<1. \tag{40}$$

The numeric solution of Eq. (7) performed in the previous subsection to find θ_∞ also gives the gap density $n(h)$. The result agrees with the radial distribution function obtained by simulation according to Eq. (40), as shown in Fig. 7 for $R^*=1$ and in Fig. 8 for $R^*=1.968$, 3.310.

V. CONCLUSIONS

A (1+1)-dimensional adsorption model has been analyzed to investigate the influence of transport mechanisms (diffusion and sedimentation) on the structure of irreversibly adsorbed monolayers of particles. We have studied a simplified model in which hard spheres suspended in a two-dimensional fluid adsorb onto a line. The results may be relevant to understand the more realistic case of adsorption on a surface, if the suggested scaling behavior between the (1+1)- and (2+1)-dimensional cases holds [21]. An argument in favor of this hypothesis for large gravity is presented below.

By means of Brownian dynamic simulations we have obtained the saturation coverage and the radial distribution function $g(r)$ for different values of the gravity number N_g. These results have been compared with those obtained from an approximate analytic formalism: first we analyze the probability density of adsorption onto a gap with the help of the transport equation and Brownian dynamic simulations; once we know this probability distribution, the saturation coverage $\theta_\infty(R^*)$ and the density of gaps at the jamming limit can be obtained numerically by using an integral equation developed in a previous paper [19].

We have introduced a superposition hypothesis, assuming that the adsorption probability at a given point depends only on the limiting particles of the gap in which the particle adsorbs. As showed by simulations, this hypothesis fails when the gap is small and $1\leqslant R^*\leqslant 2$, but this affects θ_∞ only slightly.

The probability density of adsorption in the presence of one particle was obtained by solving the transport equation as a multipolar expansion. This expansion is useful for low to intermediate N_g values, but not for high N_g numbers. In the large N_g regime we have shown, using singular perturbation techniques, that the probability density of adsorption $\rho^{(1)}(x)$ has the scaling form (29). The simulations show that this scaling is approximately satisfied even for moderate values of N_g. Instead of the exact scaling function, we have useda simple exponential function for the numerical computations that fits the simulation results. The corresponding numeric solution of the integral equation (7) agree well with the simulations even for $R^*>1$.

The properties of the adsorbed layers at jamming are as follows. For $R^*\leqslant 1$, $\theta_\infty(R^*)$ varies less than 1% and $g(r)$ is close to the DRSA ($R^*=0$) form. Therefore, the effect of gravity is nearly negligible in this regime. For $R^*\geqslant 1$, $\theta_\infty(R^*)$ grows quickly with N_g and $g(r)$ displays peaks that emerge more significantly. The peaks in $g(r)$ increase and are steeper when R^* grows reflecting the tendency of large particles to pack closer than smaller ones. For $R^*\geqslant 2.5$ the saturation coverage slowly approaches the BD value following the asymptotic expression (39). In this regime $g(r)$ is very close to its BD counterpart, although in our model $g(r)$ takes finite values at $r=1,2,\ldots$ due to the effect of diffusion instead of the delta function singularities of the BD case.

It can be easily verified that the same perturbation techniques used in Appendix B can be applied to the (2+1)-dimensional case, leading to the scaling given in Eq. (29) with the same function $\phi^{(1)}$. This fact provides a physical basis, at least for large gravity, for the scaling of $\theta_\infty(R^*)$ in a common curve for the $2+1$ and $1+1$ cases. In the asymptotic limit the relevant property of the adsorption probability is its thickness, and one can replace $\rho^{(1)}$ with a step function with the same thickness, $\Delta=kN_g^{-2/3}$ We expect that the jamming coverage approaches the ballistic limit linearly in Δ, and therefore

$$\frac{\theta_\infty(N_g\gg 1)}{\theta_\infty^{BD}}\simeq 1-\alpha_d N_g^{-2/3}, \tag{41}$$

where α_d is a constant that depends on the dimension of the system. Thus, with an adequate change of scale the curves of $\theta_\infty(N_g)/\theta_\infty^{BD}$ in $1+1$ and $2+1$ dimensions are coincident, at least for large values of N_g. This scaling has been observed in simulations and seems to apply for all values of N_g [21].

In a more realistic extension of our model, hydrodynamic interactions must be considered in the transport equation, but we expect that their effect is small. In the DRSA case, hydrodynamic interactions [22] make the adsorption probability nearly uniform due to the enhanced mobility parallel to the surface and therefore the coverage is expected to be close to the RSA case. In the case of BD it has been shown [23] that while the jamming coverage does not change significantly, the local structure is strongly affected by the hydrodynamic interactions.

Note added in proof. The authors would like to note that a similar problem has been studied by Ho Suk Choi (Ph.D. thesis, Purdue University, 1995). In this work the transport equation of a sphere diffusing in a gravitational field was solved numerically. The results are in essential agreement with those of our paper (Sec. III). The authors believe this fact should be properly represented.

ACKNOWLEDGMENTS

Useful comments by Ignacio Pagonabarraga are acknowledged. J.F. is supported by a doctoral scholarship from the Programa de formació d'investigadors of the Generalitat de Catalunya under Grant No. FI/96-2.683. We also acknowledge financial support from the Dirección General de Investigación of the Spanish Ministry of Education and Science (Grant No. PB94-0718) and the European Union under Grant No. ERBCHRXCT 920007.

APPENDIX A: MULTIPOLAR SOLUTION OF TRANSPORT EQUATION

In this appendix we obtain $\psi^{(1)}(\vec{r})$ using the Green function method. The equation and boundary conditions for $\psi^{(1)}(\vec{r})$ can be obtained by substitution of (21),(22) in (16),(17),(20). If we write $\psi^{(1)}(\vec{r})=f(\vec{r})e^{-N_g z/2}$, the equation for $f(r)$ is

$$\nabla^2 f(\vec{r})=\frac{N_g^2}{4}f(\vec{r}), \tag{A1}$$

with boundary conditions:

$$f(x,z=0)=0, \tag{A2}$$

$$\left.\frac{\partial f(\vec{r})}{\partial r}\right|_{r=1}+\frac{N_g}{2}\sin\theta f(r=1,\theta)=-\sin\theta e^{(N_g/2)\sin\theta}. \tag{A3}$$

The Green function corresponding to (A1) and satisfying the boundary condition (A2), $G(\vec{r},\vec{r}')$, is defined by

$$\nabla^2 G(\vec{r},\vec{r}')-\frac{N_g^2}{4}G(\vec{r},\vec{r}')=\delta(\vec{r}-\vec{r}'), \tag{A4}$$

$$G(x,z=0,\vec{r}')=0. \tag{A5}$$

Using the method of images, it is easy to obtain the solution to this equation, that can be expressed using Bessel functions of the third kind:

$$G(\vec{r},\vec{r}')=\frac{-1}{2\pi}\left[K_0\left(\frac{N_g}{2}|\vec{r}-\vec{r}'|\right)-K_0\left(\frac{N_g}{2}|\vec{r}-\vec{r}^*|\right)\right],$$

$$\vec{r}=(x,z),\quad \vec{r}'=(x',z'),\quad \vec{r}^*=(x',-z'). \tag{A6}$$

We can obtain an integral equation for $f(\vec{r})$ making use of the properties of the Green function. If we multiply Eq. (A1) by $G(\vec{r},\vec{r}')$ and Eq. (A4) by $-f(\vec{r})$ and add the results, we obtain:

$$G(\vec{r},\vec{r}')\nabla^2 f(\vec{r})-f(\vec{r})\nabla^2 G(\vec{r},\vec{r}')=-f(\vec{r})\,\delta(\vec{r}-\vec{r}'). \tag{A7}$$

Now, integrating (A7) over the whole volume V, limited by the adsorbing line at $z=0$, the excluded volume of the preadsorbed particle and a closing surface S, and then using the Stokes theorem, we obtain:

$$f(\vec{r}')=-\int_V dV[G(\vec{r},\vec{r}')\nabla^2 f(\vec{r})-f(\vec{r})\nabla^2 G(\vec{r},\vec{r}')]$$

$$=-\int d\vec{S}[G(\vec{r},\vec{r}')\vec{\nabla}f(\vec{r})]+\int d\vec{S}[f(\vec{r})\vec{\nabla}G(\vec{r},\vec{r}')]. \tag{A8}$$

If the surface S goes to infinity and we use the boundary conditions for f and $G(\vec{r},\vec{r}')$, the only contribution to the surface integrals comes from the excluded area of the preadsorbed particle. Therefore, using $dS=Rd\theta=d\theta$ we obtain:

$$f(\vec{r}')=\int_0^\pi d\theta\left[G(\vec{r},\vec{r}')\frac{\partial f}{\partial r}-f(\vec{r})\frac{\partial G}{\partial r}\right]_{r=1},$$

$$r'>1. \tag{A9}$$

To take profit of this expression, we use the Fourier expansion of the Green function (A6) that can be obtained using a well-known theorem for the Bessel functions [29]:

$$K_0(\beta\sqrt{r_1^2+r_2^2-2r_1r_2\cos\phi})$$

$$=\sum_{m=-\infty}^{\infty}K_m(\beta r_2)I_m(\beta r_1)\cos m\phi,$$

$$r_2\geqslant r_1. \tag{A10}$$

Use of (A10) in (A6) yields:

$$G(\vec{r},\vec{r}')=\frac{-2}{\pi}\sum_{n=1}^{\infty}K_n\left(\frac{N_g}{2}r'\right)I_n\left(\frac{N_g}{2}r\right)\sin(n\theta)\sin(n\theta'),$$

$$r\leqslant r', \tag{A11}$$

$$x=r\cos\theta,\quad z=r\sin\theta,\quad x'=r'\cos\theta',\quad z'=r'\sin\theta'.$$

Substitution of this expression in Eq. (A9) yields

$$f(\vec{r}')=-\frac{2}{\pi}\sum_{n=1}^{\infty}K_n\left(\frac{N_g}{2}r'\right)I_n\left(\frac{N_g}{2}\right)\sin(n\theta')$$

$$\times\int_0^\pi d\theta\sin(n\theta)\frac{\partial f}{\partial r}^{r=1}+\frac{2}{\pi}\sum_{n=1}^{\infty}K_n\left(\frac{N_g}{2}r'\right)$$

$$\times\frac{N_g}{4}\left[I_{n+1}\left(\frac{N_g}{2}\right)+I_{n-1}\left(\frac{N_g}{2}\right)\right]\sin(n\theta')$$

$$\times\int_0^\pi d\theta f(r$$

$$=1,\theta)\sin(n\theta). \tag{A12}$$

Now, we note that our problem is symmetric under the change $x\to\pi-x$, and, therefore, only the integrals with odd n contribute. In addition, if we apply the boundary condition of null radial flux at the excluded area defined by the preadsorbed sphere (A2) and define $\varphi(\theta)=f(r=1,\theta)$ we obtain

$$f(\vec{r}')=\frac{2}{\pi}\sum_{n=1}^{\infty}K_{2n-1}\left(\frac{N_g}{2}r'\right)\sin(2n-1)\theta'\int_0^\pi d\theta$$

$$\times\sin(2n-1)\theta\left(\sin\theta e^{(N_g/2)\sin\theta}I_{2n-1}\left(\frac{N_g}{2}\right)\right.$$

$$+\left\{\frac{N_g}{2}I_{2n-1}\left(\frac{N_g}{2}\right)\sin\theta+\frac{N_g}{4}\left[I_{2n-2}\left(\frac{N_g}{2}\right)\right.\right.$$

$$\left.\left.\left.+I_{2n}\left(\frac{N_g}{2}\right)\right]\right\}\varphi(\theta)\right). \tag{A13}$$

If we define the Fourier-sine transforms:

$$g_{2n-1}(N_g)=\int_0^\pi d\theta\,\sin(2n-1)\theta\,\sin\theta e^{(N_g/2)\sin\theta}, \tag{A14}$$

$$\Gamma_{2n-1}(N_g)=\int_0^\pi d\theta\,\sin(2n-1)\theta\,\sin\theta\varphi(\theta), \tag{A15}$$

$$\varphi_{2n-1}(N_g)=\int_0^\pi d\theta\,\sin(2n-1)\theta\varphi(\theta), \tag{A16}$$

finally one obtains for $f(r,\theta)$ (we omit $'$ for simplicity):

$$f(r,\theta)=\frac{2}{\pi}\sum_{n=1}^{\infty}\varphi_{2n-1}\frac{K_{2n-1}\left(\frac{N_g}{2}r\right)}{K_{2n-1}\left(\frac{N_g}{2}\right)}\sin(2n-1)\theta. \tag{A17}$$

By substitution of $r=1$ in (A13) and making use of definitions (A14–A16) we obtain the following equations for the coefficients φ_{2n-1}:

$$\varphi_{2n-1}=K_{2n-1}\left(\frac{N_g}{2}\right)I_{2n-1}\left(\frac{N_g}{2}\right)\times\frac{g_{2n-1}+\frac{N_g}{2}\Gamma_{2n-1}}{1-\frac{N_g}{4}K_{2n-1}\left(\frac{N_g}{2}\right)\left[I_{2n-2}\left(\frac{N_g}{2}\right)+I_{2n}\left(\frac{N_g}{2}\right)\right]}, \tag{A18}$$

$$\Gamma_{2n-1}=\frac{2}{\pi}\sum_{m=1}^{\infty}\frac{-4(2m-1)(2n-1)}{(2n+2m-3)(2n+2m-1)(2n-2m+1)(2n-2m-1)}\varphi_{2m-1}. \tag{A19}$$

The probability density for the adsorption of a particle can be obtained in a form of a multipolar expansion by using Eq. (A17) with the definition of $f(r)$, $\psi^{(1)}(\vec{r})=f(\vec{r})e^{-N_g z/2}$ in definitions (21), (23):

$$\rho(x)=1+\frac{2}{\pi|x|}\sum_{n=1}^{\infty}(2n-1)\varphi_{2n-1}\frac{K_{2n-1}\left(\frac{N_g}{2}|x|\right)}{K_{2n-1}\left(\frac{N_g}{2}\right)},\qquad |x|>1. \tag{A20}$$

For small values of N_g, one has $g_{2n-1}=(\pi/2)\delta_{n1}+O(N_g)$, and all the terms in Eq. (A20) except the first vanish to order $O(N_g)$, giving $\varphi_{2n-1}=(\pi/2)\delta_{n1}+O(N_g)$.

APPENDIX B: BOUNDARY LAYER SOLUTION OF THE TRANSPORT EQUATION

Our aim in this appendix is to obtain an approximate solution of the transport equation (16) valid for large values of N_g. When N_g is very large, the Laplacian term in the transport equation becomes negligible in the entire domain except near the boundaries, where the value of the derivatives can be large. We have then a singular perturbation problem [30]. An approximate solution in this limit can be reached by matching different approximations in the bulk and in the boundary layers that can appear near the boundaries.

The first approximation to the *outer solution* can be obtained neglecting the Laplacian term in the transport equation. The resulting equation is simply $\partial\psi/\partial z=0$, and the solution satisfying the boundary condition at infinity Eq. (17) is a constant,

$$\psi_{out}=1/N_g. \tag{B1}$$

Note that this is an exact solution of the transport equation, and therefore the expansion of the outer solution ends here.

This outer solution does not match the boundary conditions at $z=0$ and $r=1$, and therefore some boundary layers have to be introduced.

(i). A first boundary layer, appears near the line $z=0$, where the value of ψ has to change from the outer value, $1/N_g$, to the value imposed by the boundary condition, 0. Derivatives with respect to z become large, and the term $\partial^2\psi/\partial z^2$ in the Laplacian is no longer negligible. The boundary layer thickness ϵ can be estimated from the condition that the derivatives with respect to z are the dominant terms in the transport equation and have the same order. This implies $\epsilon=O(N_g^{-1})$. Therefore, the first approximation to the *inner solution* in this region is the solution of

$$\frac{\partial^2\psi_{in}^I}{\partial z^2}+N_g\frac{\partial\psi_{in}^I}{\partial z}=0. \tag{B2}$$

The solution satisfying the boundary condition at $z=0$ and matching the outer solution for $z\gg N_g^{-1}$ is

$$\psi_{in}^I=\frac{1}{N_g}(1-e^{-N_g z}). \tag{B3}$$

This is also an exact solution of the transport equation, so the expansion of the inner solution in this boundary layer ends

here. In the absence of any adsorbed particle, no additional boundary layers are present and, in fact, we have reproduced the exact solution for an empty line given by Eq. (22).

(ii). In the presence of one particle in $r=0$, a new boundary layer appears near the boundary of that particle, $r=1$. The function ψ has to change in a small boundary of thickness δ from the outer form (B1), in which there is a radial probability flux, to a form in which that flux vanishes at $r=1$. The order of magnitude of the different terms of the transport equation can be easily evaluated by writing it in polar coordinates, and considering that each radial derivative introduces a factor $O(\delta^{-1})$:

$$\frac{\partial^2\psi}{\partial r^2} + \frac{1}{r}\frac{\partial\psi}{\partial r} + \frac{1}{r^2}\frac{\partial^2\psi}{\partial\theta^2} + N_g\sin\theta\frac{\partial\psi}{\partial r} + N_g\frac{\cos\theta}{r}\frac{\partial\psi}{\partial\theta} = 0.$$

$$O(\delta^{-2})\ O(\delta^{-1})\ O(1) \qquad O(N_g\delta^{-1}) \qquad O(N_g) \tag{B4}$$

The first and fourth terms of this equation are the largest when $N_g\to\infty$, and the appropriate *distinguished limit* is obtained when they have the same order of magnitude, that is, when $\delta=O(N_g^{-1})$. To obtain the solution in this boundary layer, we define the scaled inner variable $\eta\equiv N_g(r-1)$, and we expand the function ψ_{in}^{II} in successive approximations, $\psi_{in}^{II}=\psi^{(1)}+\psi^{(2)}+\cdots$. The first approximation to the inner solution is then, retaining the terms of order $O(N_g^2)$,

$$\frac{\partial^2\psi^{(1)}}{\partial\eta^2} + \sin\theta\frac{\partial\psi^{(1)}}{\partial\eta} = 0. \tag{B5}$$

The boundary conditions for $\psi^{(1)}$ cause the normal flux to vanish at $\eta=0$ and the solution has to match the outer solution for $\eta\to\infty$. The first integral of Eq. (B5) is immediate,

$$\frac{\partial\psi^{(1)}}{\partial\eta} + \sin\theta\psi^{(1)} = C(\theta). \tag{B6}$$

The term on the right-hand side is an integration constant that, in principle, can be an arbitrary function of θ. However, the left hand side is proportional to the radial flux and, by the boundary condition at $\eta=0$, the integration constant must vanish. We have, then, a homogeneous first-order equation for $\psi^{(1)}$, whose general solution is

$$\psi^{(1)} = A(\theta)e^{-\eta\sin\theta}. \tag{B7}$$

It is not possible to obtain the ''integration constant'' $A(\theta)$ by direct matching with the outer solution, because this first approximation to the inner solution vanishes when $\eta\to\infty$. As we will see, the reason for this is that the first approximation $\psi^{(1)}$ is a quantity of order $\mathcal{O}(1)$, whereas the outer solution is $\mathcal{O}(N_g^{-1})$. Matching is possible only for the second-order approximation, $\psi^{(2)}$, which is $\mathcal{O}(N_g^{-1})$. Retaining terms of order $\mathcal{O}(N_g)$ in the transport equation we obtain the equation satisfied by $\psi^{(2)}$,

$$\frac{\partial^2\psi^{(2)}}{\partial\eta^2} + \sin\theta\frac{\partial\psi^{(2)}}{\partial\eta} = -N_g^{-1}\left(\frac{\partial\psi^{(1)}}{\partial\eta} + \cos\theta\frac{\partial\psi^{(1)}}{\partial\theta}\right)$$
$$= -N_g^{-1}\cos\theta e^{-\eta\sin\theta} \times[A'(\theta)-A(\theta)(\eta\cos\theta+\tan\theta)]. \tag{B8}$$

The first integral satisfying the boundary condition at $\eta=0$ is

$$\frac{\partial\psi^{(2)}}{\partial\eta} + \sin\theta\psi^{(2)} = -N_g^{-1}\cos\theta\int_0^\eta d\eta' e^{-\eta'\sin\theta} \times[A'(\theta)-A(\theta)(\eta'\cos\theta+\tan\theta)]. \tag{B9}$$

It is not necessary to go beyond this calculation to obtain the matching condition with the outer solution. It suffices to recognize that the left-hand side of the last equation is $-N_g^{-1}$ times the radial probability flux, and this quantity has to match when $\eta\to\infty$ with the outer value for this flux, which from (B1) is simply $-\sin\theta$. We obtain the condition:

$$-\sin\theta = \cos\theta\left\{\frac{A'(\theta)-A(\theta)\tan\theta}{\sin\theta} - \frac{A(\theta)\cos\theta}{\sin^2\theta}\right\}. \tag{B10}$$

This is a differential equation for the unknown function $A(\theta)$, whose general solution is $A(\theta)=\sin\theta+B\tan\theta$. The arbitrary constant B has to vanish in order to obtain a finite probability density for $\theta=\pi/2$. This completely determines the first approximation to ψ_{in}^{II}

However, this approximate solution is not valid for all values of the angle θ. The reason is that the boundary layer thickness is $\delta=(N_g\sin\theta)^{-1}$, as is evident from Eq. (B7), and it increases with decreasing angle. Therefore, the boundary layer approximation breaks down when $\theta\to0$. It is easy to verify that the order of magnitude of the last term on the left-hand side of Eq. (B4), which has been neglected, becomes comparable to the retained terms when $\theta=\mathcal{O}(N_g^{-1/3})$. Therefore, the range of validity of the solution obtained is

$$\psi_{in}^{II} = \sin\theta e^{-\eta\sin\theta} + O(N_g^{-1}), \quad \theta\gg N_g^{-1/3}. \tag{B11}$$

(iii). For values of the angle $\theta=O(N_g^{-1/3})$, the last term in Eq. (B4) has to be included in the boundary layer equation together with the two terms retained in the previous approximation. All these terms have the same order of magnitude when the radial thickness of the boundary layer is $\delta=\mathcal{O}(N_g^{-2/3})$. These range of values for the angle and the radius define a new boundary layer; we introduce new appropriately scaled variables, $\xi=(r-1)N_g^{2/3}$ and $\tau=\theta N_g^{1/3}$. We introduce also an asymptotic expansion of the probability density, $\psi_{in}^{III}=\mu_1(N_g)\phi^{(1)}+\mu_2(N_g)\phi^{(2)}+\cdots$, where the coefficients $\mu_i(N_g)$ are infinitesimals of increasing order. The equation for $\phi^{(1)}$ is, retaining the terms of larger order in N_g:

$$\frac{\partial \phi^{(1)}}{\partial \tau}+\frac{\partial^2 \phi^{(1)}}{\partial \xi^2}+\tau\frac{\partial \phi^{(1)}}{\partial \xi}=0. \tag{B12}$$

We now have a parabolic equation that has the form of a time-reversed diffusion equation with a drift proportional to the ''time'' τ. For $\tau\to\infty$, the solution has to match with the previous boundary layer solution ψ_{in}^{II} valid for large values of the angle. It is easy to see that this implies

$$\mu_1(N_g)=N_g^{-1/3},$$

$$\phi^{(1)}\to \tau e^{-\tau\xi}, \quad \tau\to+\infty. \tag{B13}$$

That is, for large values of τ we recover a normalized ''Boltzmann distribution,'' corresponding to neglecting the τ derivative in Eq. (B12). This condition, together with the boundary of condition of zero normal flux at $\xi=0$, $\partial\phi^{(1)}/\partial\xi+\tau\phi^{(1)}=0$, completely specifies the function $\phi^{(1)}$. Furthermore, the condition of zero flux at $\xi=0$, implies that the integral of $\phi^{(1)}$ with respect to ξ is a conserved quantity, and as a consequence of Eq. (B13) it has value 1:

$$\int_0^\infty \phi^{(1)}(\xi,\tau)d\xi=1. \tag{B14}$$

We have not been able to analytically solve Eq. (B12). However, it is easy to obtain a numeric solution satisfying the cited boundary conditions. The solution is a positive normalized function, vanishing exponentially for $\xi\to\infty$, and with a well-defined limit when $\tau\to0$, $\phi^{(1)}(\xi,\tau=0)$ (see Fig. 4). An important quantity is its first moment, $A=\int_0^\infty d\xi\xi\phi^{(1)}(\xi)=1.106\ldots$.

The adsorbing boundary condition at $z=0$, however, is still not satisfied by this approximation. From the previous solution we have $\lim_{\tau\to0}\psi=N_g^{-1/3}\phi^{(1)}(\xi,0)$ and this result, obtained from an approximation valid for $\theta=O(N_g^{-1/3})$, has to be modified to agree with the boundary condition $\psi(\theta=0)=0$. Indeed, when $\theta=O(N_g^{-1})$, we are in the same situation as in the boundary layer (I): the derivatives with respect to θ are of order $\epsilon=O(N_g^{-1})$, and the boundary layer equation is Eq. (B2). The range of validity of the boundary layer approximation ψ_{in}^{III} is therefore

$$\psi_{in}^{III}=N_g^{-1/3}\phi^{(1)}(\xi,\tau), \quad N_g^{-1}\ll\theta\ll1. \tag{B15}$$

(iv). A new boundary layer is needed for $\theta=O(N_g^{-1})$, in which the approximate transport equation is Eq. (B2). The solution of that equation satisfying the boundary condition at $\theta=0$ is

$$\psi_{in}^{IV}\simeq C(\xi)(1-e^{-N_g\theta}). \tag{B16}$$

The arbitrary function $C(\xi)$ is obtained by imposing matching with the approximate solution in the previous boundary layer $\psi_{in}^{(III)}$ We obtain

$$\psi_{in}^{IV}(r,\theta)\simeq N_g^{-1/3}\phi^{(1)}(\xi,\tau=0)(1-e^{-N_g\theta}), \quad \theta\ll N_g^{-1/3}. \tag{B17}$$

This function gives the correction to the probability flux, originated from the presence of the fixed particle, $\rho^{(1)}$:

$$\rho^{(1)}(r)\equiv\left.\frac{\partial\psi}{\partial z}\right|_{z=0}\simeq N_g^{2/3}\phi^{(1)}(\xi,\tau=0), \quad \xi=(r-1)N_g^{2/3}. \tag{B18}$$

Therefore, the numerical solution of Eq. (B12) specifies the final probability distribution. One important conclusion is that, for large values of N_g, $\rho^{(1)}$ scales to a function of the form $N_g^{2/3}\phi^{(1)}[(r-1)N_g^{2/3}]$. It is easy to verify, using Eq. (B14), that this distribution is normalized,

$$\int_1^\infty \rho^{(1)}(r)dr=\int_0^\infty \phi^{(1)}(\xi,\tau=0)d\xi=1. \tag{B19}$$

[1] Z. Adamczyk, B. Siwek, M. Zembala, and P. Belouschek, Adv. Colloid Interface Sci. **48**, 151 (1994).
[2] J. Feder and I. Giaever, J. Coll. Interface Sci. **78**, 144 (1980).
[3] J. J. Ramsden, Phys. Rev. Lett. **71**, 295 (1993).
[4] G. Y. Onoda and E. G. Liniger, Phys. Rev. A **33**, 715 (1986).
[5] P. Wojtaszczyk, P. Schaaf, B. Senger, M. Zembala, and J.-C. Voegel, J. Chem. Phys. **99**, 7198 (1993).
[6] J. W. Evans, Rev. Mod. Phys. **65**, 1281 (1993).
[7] A. Rènyi, Sel. Trans. Math. Stat. Prob. **4**, 205 (1963); E. R. Cohen and H. Reiss, J. Chem. Phys. **38**, 680 (1963); B. Widom, *ibid.* **44**, 2888 (1966); J. J. Gonzalez, P. C. Hemmer, and J. S. Høye, Chem. Phys. **3**, 288 (1974).
[8] Y. Pomeau, J. Phys. A **13**, L193 (1980); R. H. Swendsen, Phys. Rev. A **24**, 504 (1981).
[9] E. L. Hinrichsen, J. Feder, and T. J. Jøssang, J. Stat. Phys. **44**, 793 (1986).
[10] B. Bonnier, D. Boyer, and P. Viot, J. Phys. A 27, 3671 (1994).
[11] G. Tarjus, P. Schaaf, and J. Talbot, J. Chem. Phys. **93**, 8352 (1990); D. Boyer, G. Tarjus, P. Viot, and J. Talbot, J. Chem. Phys. **103**, 1607 (1995).
[12] G. Tarjus, P. Schaaf, and J. Talbot, J. Stat. Phys. **63**, 167 (1991).
[13] T. G. M. van de Ven, *Colloidal Hydrodynamics* (Academic Press, New York, 1989).
[14] R. Jullien and P. Meakin, J. Phys. A **25**, L189 (1992); A. P. Thompson and E. D. Glandt, Phys. Rev. A **46**, 4639 (1992); H. S. Choi, J. Talbot, G. Tarjus, and P. Viot, J. Chem. Phys. **99**, 9296 (1993).
[15] J. Talbot and S. M. Ricci, Phys. Rev. Lett. **68**, 958 (1992).
[16] P. Viot, G. Tarjus, and J. Talbot, Phys. Rev. E **48**, 480 (1993).
[17] P. Schaaf, A. Johner, and J. Talbot, Phys. Rev. Lett. **66**, 1603 (1991); B. Senger, J.-C. Voegel, P. Schaaf, A. Johner, A. Schmitt, and J. Talbot, Phys. Rev. A **44**, 6926 (1991); B. Senger, P. Schaaf, J.-C. Voegel, A. Johner, A. Schmitt, and J. Talbot, J. Chem. Phys. **97**, 3813 (1992); B. Senger, J. Talbot, P. Schaaf, A. Schmitt, and J.-C. Voegel, Europhys. Lett. **21**, 135 (1993).
[18] D. L. Ermak and J. A. McCammon, J. Chem. Phys. **69**, 1352 (1978).

[19] F.J. Bafaluy, H.S. Choi, B. Senger, and J. Talbot, Phys. Rev E **51**, 5985 (1995).

[20] B. Senger, J. Bafaluy, P. Schaaf, A. Schmitt, and J.-C. Voegel, Proc. Natl. Acad. Sci. USA **89**, 9449 (1992); B. Senger, R. Ezzedine, J. Bafaluy, P. Schaaf, F. J. G. Cuisinier, and J.-C. Voegel, J. Theor. Biol. **163**, 457 (1993);

[21] R. Ezzeddine, P. Schaaf, J.C. Voegel, and B. Senger, Phys. Rev. E **51**, 6286 (1995).

[22] J. Bafaluy, B. Senger, J.-C. Voegel, and P. Schaaf, Phys. Rev. Lett. **70**, 623 (1993).

[23] I. Pagonabarraga and J.M. Rubí, Phys. Rev. Lett. **73**, 114 (1994).

[24] J. Faraudo and J. Bafaluy (unpublished).

[25] R. Ezzedine, P. Schaaf, J.-C. Voegel, and B. Senger, Phys. Rev. E **53**, 2473 (1996).

[26] J.P. Hansen and I.R. McDonald *Theory of Simple Liquids* (Academic Press, London, 1990).

[27] P. Schaaf, P. Wojtaszczyk, E. K. Mann, B. Senger, J.-C. Voegel, and D. Bedeaux, J. Chem. Phys. **102**, 5077 (1995).

[28] B. Lavenda, *Statistical Physics: A Probabilistic Approach*, (Wiley & Sons, New York, 1991).

[29] M. Abramowitz and I. Stegun, *Handbook of Mathematical Functions* (Dover, New York, 1970).

[30] J. Kevorkian and J. D. Cole, *Perturbation Methods in Applied Mathematics* (Springer, New York, 1980).